Sādhanā Vol. 42, No. 8, August 2017, pp. 1377–1387
DOI 10.1007/s12046-017-0656-2

Impedance estimation of photovoltaic modules for inverter start-up analysis

PALLAVI BHARADWAJ*, ABHIJIT KULKARNI and VINOD JOHN

Department of Electrical Engineering, Indian Institute of Science, Bangalore 560012, India
e-mail: bharadwaj@ee.iisc.ernet.in

MS received 30 March 2016; revised 15 July 2016; accepted 9 August 2016

Abstract. Starting-up of photovoltaic (PV) inverters involves pre-charging of the input dc bus capacitance. Ideally, direct pre-charging of this capacitance from the PV modules is possible as the PV modules are current limited. Practically, the parasitic elements of the system such as the PV module capacitance, effective wire inductance and resistance determine the start-up transient. The start-up transient is also affected by the contactor connecting the PV modules to the inverter input dc bus. In this work, the start-up current and voltages are measured experimentally for different parallel and series connections of the PV modules. These measurements are used to estimate the stray elements, namely the PV module capacitance, effective inductance and resistance. The estimation is based on a linear small-signal model of the start-up conditions. The effect of different connections of the PV modules and the effect of varying irradiation on the scaling of the values of the stray elements are quantified. The System model is further refined by inclusion of connecting cable capacitance and contactor resistance. Dynamics of the resulting fifth-order model are seen to be consistent with those of the simplified third-order model. The analysis of this paper can be used to estimate the expected peak inrush current in PV inverters. It can also be used to arrive at a detailed modelling of PV modules to evaluate the transient behaviour.

Keywords. Photovoltaic module; dynamic model; solar cell capacitance; cable impedance; irradiation-dependence.

1. Introduction

Photovoltaic (PV) cell capacitance measurement has drawn attention of researchers in recent times owing to the importance of dynamically modelling a PV panel when it interacts with switching converters. Capacitance affects the maximum power point tracking of PV panels [1]. It also causes the flow of inrush current, when a power converter connected to PV is turned on. If the inrush current is large, it can damage the devices of the converter and components such as safety fuses. To prevent the flow of large inrush current, many pre-charge techniques are discussed in literature [2]. The PV panel parasitic capacitance decides the amount of leakage current to ground and therefore may impact the safety of operating professionals [3]. PV capacitance can be theoretically estimated using p–n junction parameters such as doping [4]. Parasitic capacitance to ground can be analytically estimated using the fringe capacitor model [3]. Many methods of experimental evaluation of PV panel's capacitance are reported in literature, such as impedance spectroscopy [4–7], voltage ramp method [8–10] and transient response measurement [1]. Impedance spectroscopy involves superposition of an ac small signal over a dc bias voltage. The frequency of the ac signal is varied from a few hertz to hundred kHz and the impedance is measured. Often PV impedance measurement experiments reported in literature are performed in dark, with voltage applied externally [4–7]. This, however, does not reflect the true picture because junction condition is not the same for an irradiated PV panel as compared with a dark panel with voltage applied. Many papers report measurement of capacitance using a reverse dc bias across the solar cell. This again will not give the capacitance of an operating solar cell, as capacitance depends on voltage and a solar cell normally operates under zero bias. As capacitance varies with illumination, voltage and type of solar cell, for a specific application, under given light and bias conditions, it is best determined experimentally. In [1], an external capacitor is connected across a PV panel. The transient current waveform is used to estimate L and C values. However, the first current peak is truncated and the second and third current peak's magnitude and time are used to calculate the parameters. The resultant values of inductance and capacitance parameters, as reported in [6]

*For correspondence

to be 0.05 μF/cm^2 capacitance for polycrystalline panels, are inconsistent with practical values.

In the present work, the PV module impedance is evaluated from the perspective of evaluating the pre-charge current that can occur in a PV array when an inverter dc bus is connected. For this, the experimentally obtained current response is analysed as a simplified second-order model. This model is compared to a small-signal model of the actual non-linear PV circuit. The values of parameters estimated are seen to be in agreement with practical values, as reported in literature for polycrystalline PV panels [6]. Also, the variation of PV module capacitance with voltage and irradiation is quantified for the present system. Scaling up of capacitance with different series and parallel connections of PV modules to form arrays is studied, along with the effect of cable impedance. The cable impedance model is further improved by incorporating the effect of cable capacitance in an equivalent Π model. Study of this equivalent impedance is crucial to determine the terminal voltage and inrush current, as faced by a power electronic converter, connected to the PV system.

This paper is divided into six sections. The system model consisting of the modules, cable and inverter is discussed in section 2. In section 3, experimental results are discussed. Limitations of extending the PV modules analysis to a generic PV array are discussed in section 4. Section 5 discusses the improved model with equivalent Π representation of the connecting cable. Section 6 concludes the paper.

2. System model

Consider the circuit shown in figure 1. It shows the dynamic equivalent circuit of a PV module array, connected through a cable having a resistance, R_c, and inductance, L_c, to a converter having a dc bus capacitance, C_{inv}.

In the PV array model, I_g represents the light-induced current in the PV module, and I_o represents the diode dark saturation current and m is the diode ideality factor. R_{sh} and R_s are, respectively the shunt and series resistance, modelling the loss of power within the solar cells of the array. Capacitance C models the combined effect of the cell junction and diffusion capacitance, as well as the parasitic capacitance of positive and negative terminals of the PV module to the ground.

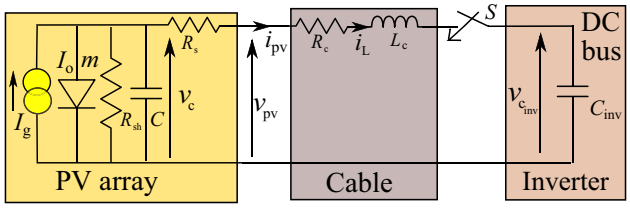

Figure 1. PV array dynamic model, connected to the dc bus of an inverter, via a connecting cable.

Combined series resistance is represented by $R = R_s + R_c$, and series inductance is represented by $L = L_c$. The KCL and KVL equations for the circuit shown in figure 1 are

$$i_L = I_g - I_o\left(e^{\frac{v_c}{mn_sV_T}} - 1\right) - \frac{v_c}{R_{sh}} - C\frac{dv_c}{dt}, \tag{1}$$

$$v_c = i_L R + L\frac{di_L}{dt} + v_{c_{inv}}, \tag{2}$$

$$i_L = C_{inv}\frac{dv_{c_{inv}}}{dt}. \tag{3}$$

2.1 *Small-signal model*

Let $\bar{x} = [v_c, i_L, v_{c_{inv}}]'$. Then these equations can be rewritten in the form $\dot{\bar{x}} = f(\bar{x})$ as follows:

$$\frac{dv_c}{dt} = -\frac{i_L}{C} - \frac{v_c}{CR_{sh}} - \frac{I_o e^{\frac{v_c}{mn_sV_T}}}{C} + \frac{I_g + I_o}{C}, \tag{4}$$

$$\frac{di_L}{dt} = -\frac{R}{L}i_L + \frac{v_c}{L} - \frac{v_{c_{inv}}}{L}, \tag{5}$$

$$\frac{dv_{c_{inv}}}{dt} = \frac{i_L}{C_{inv}}. \tag{6}$$

This can further be linearised into the form $\dot{\bar{x}} = A\bar{x}$ for a linear time invariant system. It can be seen that due to the presence of a diode, Eq. (4) is non-linear. As the dc bus capacitance C_{inv} is large, its voltage takes time to build up. The circuit emulates a short-circuit condition on the PV panel, and this time interval can be considered as a quasi-equilibrium, which is perturbed by LC oscillations. If a small-signal analysis is performed to analyse this perturbation, the evaluated partial derivatives, written in the matrix form (7), result in a linear system about the equilibrium condition:

$$\Delta\dot{\bar{x}} = \begin{bmatrix} -\frac{1}{CR_{sh}} - \frac{I_o e^{\frac{v_c}{mn_sV_T}}}{Cmn_sV_T} & -\frac{1}{C} & 0 \\ \frac{1}{L} & \frac{-R}{L} & -\frac{1}{L} \\ 0 & \frac{1}{C_{inv}} & 0 \end{bmatrix} \times \Delta\bar{x}. \tag{7}$$

Another way of arriving at the linear system is by considering only the loops consisting of the linear RLC elements in figure 1, which result in oscillatory circuit response, as shown in figure 2. Writing KVL and KCL equations for this circuit, and rearranging into a state space form, one can obtain

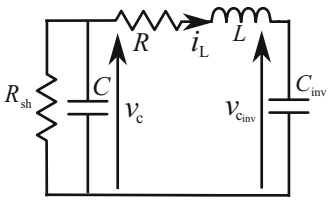

Figure 2. Simplified circuit showing only linear passive components including three energy storing elements.

$$\dot{\bar{x}} = \begin{bmatrix} -\frac{1}{CR_{sh}} & -\frac{1}{C} & 0 \\ \frac{1}{L} & \frac{-R}{L} & -\frac{1}{L} \\ 0 & \frac{1}{C_{inv}} & 0 \end{bmatrix} \times \bar{x}. \tag{8}$$

The difference between (8) and (7) is the (1,1) term in RHS matrix. If this term is negligible for the obtained parameter values, the simplified model from figure 2 can be used to represent the non-linear model from figure 1.

2.2 *Simplified second-order model*

To analyse the response of the circuit shown in figure 2, it is analysed in Laplace domain. It must be noted that the presence of R_{sh} makes the circuit in figure 2 a third order system. As the value of R_{sh} is large, it can be ignored, and the circuit can be further simplified to a second-order system.

Initially the PV terminals are assumed to be open-circuited, and external capacitor is assumed to be uncharged. Therefore, initial conditions for both inductor current and external capacitor voltage remain zero, i.e. $i_L(0) = 0$ A, $v_{c_{inv}} = 0$ V. However the PV panel capacitor is charged to the open-circuit voltage initially, $v_c = V_{oc}$. Inductor current can be written as follows:

$$I_L(s) = \frac{V_{oc}/L}{s^2 + s(R/L) + \frac{1}{LC_s}} \tag{9}$$

where C_s is the series equivalent capacitance, given by the relation

$$\frac{1}{C_s} = \frac{1}{C} + \frac{1}{C_{inv}}. \tag{10}$$

The time domain solution of (9) can be obtained as

$$i_L(t) = \frac{V_c}{\omega_d L} e^{-\zeta\omega_n t} \sin(\omega_d t), \tag{11}$$

where

$$\omega_n = \frac{1}{\sqrt{LC_s}}, \tag{12}$$

$$\zeta = \frac{R}{2\omega_n L}, \tag{13}$$

$$\omega_d = \omega_n \sqrt{1 - \zeta^2}. \tag{14}$$

Let the first current peak occur at time t_1 and the second peak occur at time t_2. Since the angle difference between the two consecutive sinusoidal peaks is taken as 2π, ω_n in terms of $\tau_s = t_2 - t_1$ can be written as (15). From measurements, τ_s is known and ω_n can be evaluated; Eq. (12) provides a relationship constraint between L and C_s.

$$\omega_n = \frac{2\pi}{\tau_s \sqrt{1 - \zeta^2}}. \tag{15}$$

2.3 *Inductance calculation*

At time $t = 0$, the current flowing through inductor L is zero and voltage across capacitor C is equal to the open-circuit voltage. As the initial voltage across external capacitor C_{inv} and resistor R is equal to zero, total voltage v_c comes across the inductor; this can be used to determine L as follows:

$$L \frac{di_L}{dt}\bigg|_{t=0} = v_c\bigg|_{t=0}. \tag{16}$$

Thus, if the initial slope is known along with initial PV capacitor voltage, then L can be computed.

2.4 *Resistance calculation*

Once the oscillation in the transient response has died down and the current has become constant, the voltage drop across the inductor becomes zero, while the voltage across the external capacitor is still negligible; thus all the voltage is dropped across the resistor, which can be evaluated as follows:

$$R = \frac{v_C}{i_L}\bigg|_{\tau_F} \tag{17}$$

where τ_F corresponds to a time when the oscillations have died down. Voltage build-up on C_{inv} can be written as

$$v_{c_{inv}} \cong \frac{I_{sc} \times t}{C_{inv}} \tag{18}$$

if $\tau_F \ll \frac{V_{oc} \times C_{inv}}{I_{sc}}$ then it can be approximated that $v_{c_{inv}} \cong 0$. If the voltage measurements are made at the cable connection point, marked as v_{pv} in figure 1, then the measured resistance in (17) would correspond to R_c and not R.

2.5 *Capacitance calculation*

From (12) to (15), capacitance can be evaluated as follows:

$$C_s = \frac{1}{L\left(\left(\frac{2\pi}{\tau_s}\right)^2 + \left(\frac{R}{2L}\right)^2\right)}. \tag{19}$$

In (19), R, L and τ_s are substituted to obtain the equivalent capacitance value of the series R–L–C circuit. For a linear series R–L–C circuit, the frequency of oscillations should remain fixed as shown in figure 3. However, in the case of PV inrush current, with the change in terminal voltage, from open circuit to short circuit, PV capacitance changes, resulting in unequal time intervals between the first two peaks as compared with the subsequent peaks, as discussed in section 3.5. Since external capacitor C_{inv} is known, from C_s, PV capacitance C can be obtained as

$$C = \frac{C_s C_{inv}}{C_{inv} - C_s}. \tag{20}$$

2.5a *Scaling up*: If this capacitance C obtained is for a single panel, then it can be scaled up for a PV panel array consisting of several series and parallel connected panels. The method used to find equivalent capacitance is similar to finding the equivalent series and parallel resistances of PV array [11]. If there are N_s panels in series forming one string and N_p such strings in parallel, C_{eq} is given by the relation

$$C_{eq} = \frac{N_p}{N_s} C. \tag{21}$$

Here it is assumed that all the PV panels are identical and therefore have equal capacitance. For an array of PV panels, the capacitance C should be replaced by C_{eq} in all these derived expressions.

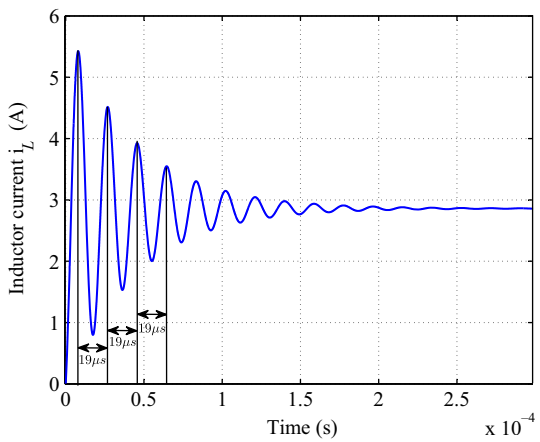

Figure 3. Simulated current waveform for a linear series $R-L-C$ circuit, showing equal time intervals between subsequent peaks.

3. Experimental results and discussion

3.1 *System under study*

The system under study comprises 14 polycrystalline PV panels, each rated at 300 W, 40 V. These panels can be connected in different series and parallel combinations. In this paper, five configurations are considered, as follows: I – single panel, II – two panels in series, III – seven parallel panels, IV – seven parallel panels in series with seven parallel panels and V – fourteen parallel panels.The array capacitance is measured by the current response of the circuit when an external capacitor is connected. The connection is made using a mechanical switch shown as MCB [12] in figure 4. It must be noted that the response is different when a solid-state switch is used. In a practical scenario a mechanical switch makes and breaks the contact, and therefore is analysed in the present study.

3.1a *Single PV panel*: For a single 300 W polycrystalline PV panel, measurements are shown in figure 5a and b. The complete response is provided together, with figure 5a captured in μs time scale and figure 5b captured in ms time scale. In figure 5, the measurements are taken at PV array terminals as indicated by the roof bus bar in figure 4. Based on the discussion in section 2 and using the experimental

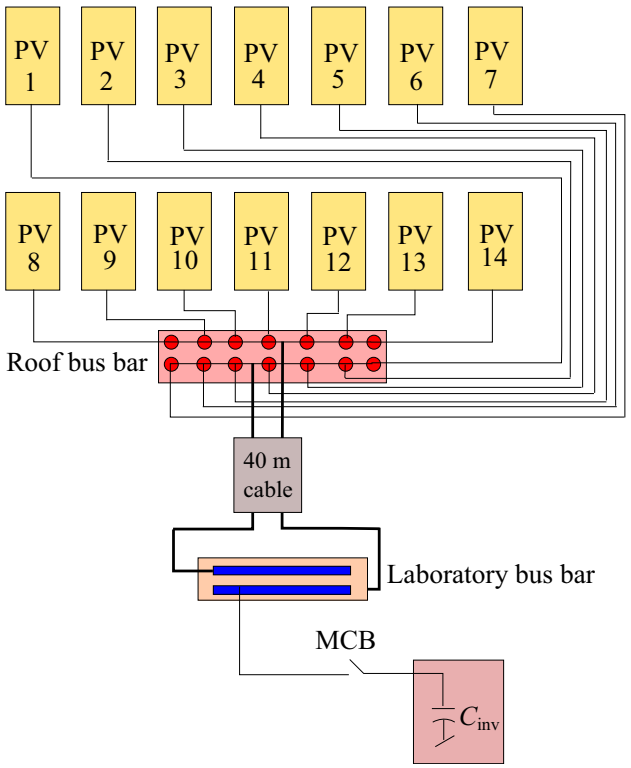

Figure 4. Single-line diagram of the installed PV system, consisting of 14 × 300 W polycrystalline PV panels, connected via cables and bus bar to a 33 mF capacitor through a circuit breaker.

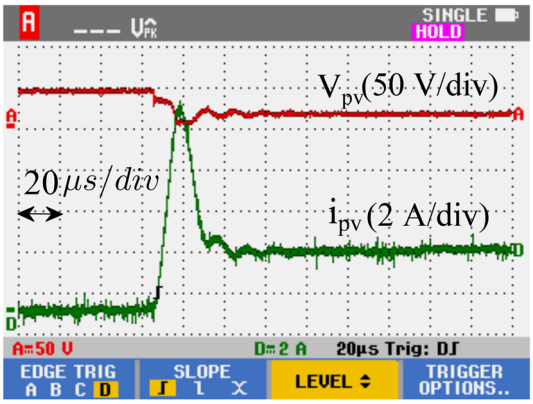

(**a**)

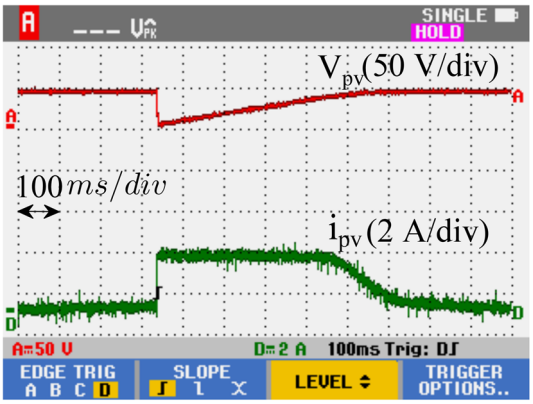

(**b**)

Figure 5. Measured PV array terminal voltage (Channel-A) and current (Channel-D) of a PV panel when connected to a capacitor (**a**) in μs time scale and (**b**) in ms time scale, for a single 300 W PV panel.

result shown in figure 5a, the resistance is computed to be 4 Ω from the dc portion of the curve. Inductance value can be evaluated from the initial slope of the current curve as shown in figure 5a. Its value is calculated to be 86 μH. By noting the time periods between successive peaks, it can be observed that damped frequency of the system changes. For a linear system, as the damped frequency is a function of R, L and C, it should remain fixed. However, in this case it changes. This is due to the change in PV module capacitance with voltage [6]. Due to charging of external capacitance, PV panel voltage changes from open-circuit voltage to zero, at the instant of closing of switch S in figure 1, as shown in figure 5b. This causes a corresponding change in panel capacitance. It can be further observed from figure 5a that the time difference between the first two peaks is significantly higher than that of successive peaks, for which it is almost constant. Thus, a major change in capacitance occurs only initially, when voltage changes significantly. For this case, capacitance comes out to be 104 nF from first two peaks and 60 nF from second and third peak time difference. It remains almost the same for successive peaks. It should be noted that $\frac{R^2}{4L}$ term is much smaller as compared with $\frac{4\pi^2 L}{\tau_s^2}$, and capacitance can be directly approximated as $C = \frac{\tau_s^2}{4\pi^2 L}$ in (19). Also, it must be noted that PV panel capacitance is in nF range, which is much smaller than the 33 mF external capacitor C_{inv}; therefore the series combination of these two is almost equal to PV capacitance, i.e. $C_s \cong C$.

3.2 *Validation of the simplified second-order model*

As mentioned in section 2.1, to validate the values of the estimated parameters: R, L and C, the model needs to be validated. The difference between the R–L–C series model and the small-signal model of the overall non-linear solar cell model, is the (1,1) term of the RHS matrix in (7) and (8). As mentioned in section 2.2, R_{sh} is also ignored to simplify the system to a second-order system; therefore, for validation, the effect of R_{sh} will also be included in the (1,1) term. Evaluating this term using the parameters evaluated for the experimental system, by substituting C = 104 nF, I_o = 0.36 μA [13], m = 1.3 [13], R_{sh} = 340 Ω, n_s = 72 [14] and V_T = 26 mV, the difference term comes out to be

$$-\frac{1}{CR_{sh}} - \frac{I_o e^{\frac{v_c}{mn_s V_T}}}{Cmn_s V_T} = -28.3 \times 10^3 - 1.42e^{\frac{v_c}{2.43}}. \quad (22)$$

Assuming that voltage drop across PV array series resistance is negligible, PV capacitance voltage would be approximately equal to the PV array terminal voltage. Substituting $v_c = 15$ V from figure 5a and writing the complete equation for $\dot{v}_c$ from (7) and (22) gives

$$\dot{v}_c = (-28.3 \times 10^3 - 1.7 \times 10^3)\Delta v_c + 9.6 \times 10^6 \Delta i_L. \quad (23)$$

From (23) it can be seen that the influence of Δi_L term is much more significant, as compared with the Δv_c term, for practical start-up conditions of inverter pre-charge. It can be noted that v_c falls to zero during the pre-charge duration. It is seen that the difference between the small-signal model and the simplified second-order model is insignificant for small values of v_c. It can be observed from figure 5a to be true because when the capacitor voltage rises to a significant value, the oscillations subside. Thus the simplified second-order model can be used to estimate the parameters of the PV module as suggested in section 2.

3.2a *Other PV array configurations*: Experimental response for various configuration of PV modules were recorded such as two panels connected in series, seven panels connected in parallel and seven parallel in series with seven parallel panels. Current and voltage response for the seven parallel panels case is shown in figure 6. Resulting cable resistance and inductance values along with panel capacitance values are tabulated in table 1. It can be observed that

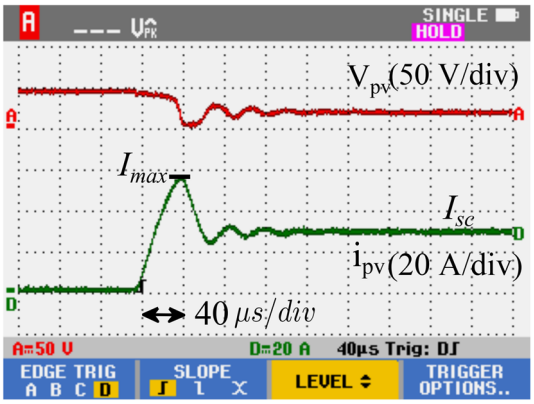

(a)

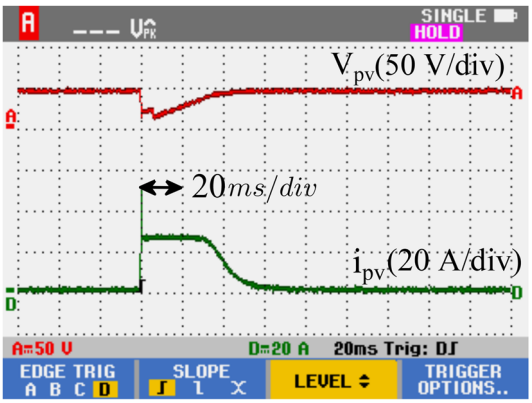

(b)

Figure 6. Measured terminal voltage (Channel-A) and current (Channel-D) of a PV panel when connected to a capacitor (**a**) in μs time scale and (**b**) in ms time scale, for seven 300 W PV panels connected in parallel

Table 1. Measured resistance, inductance and capacitance values for different PV array configurations.

Array	R (Ω)	L (μH)	C_{eq} (nF)
I	4	86	60
II	7	201	30
III	0.6	45	600
IV	1	94.6	222

series connection doubles the inductance and resistance, and halves the capacitance value, and vice-versa for parallel connection. However the scaling is not exact; this is due to the effect of cable inductance and capacitance, which connect PV panels to the bus bars, where the measurements are taken.

3.3 *Effect of cable inductance on scaling*

Cable inductance, from roof bus bar to laboratory bus bar, as indicated in figure 4, was measured to be 16 μH by an LCR meter. Subtracting this value from the overall inductance value, as reported in table 1, the roof top panel inductance can be calculated. For single panel case it comes out to be 70 μH from table 1. For the second case, series connection is done in the laboratory; therefore subtracting 2×16 μH from 201, 169 μH is obtained. This is seen to be more than double the value for the single panel owing to the mutual coupling between the cables running from roof to laboratory. For the seven-parallel case, subtracting 16 μH, 29 μH is obtained, which is more than $70/7 = 10$ μH; this is due to mutual coupling among connecting cables on the roof as shown in figure 4. For seven parallel-panels in series with seven parallel panels case, inductance is slightly more than double of the seven-parallel case inductance This again is due to the mutual coupling effect, which is missing in the seven-parallel case, as only one set of cable is energised.

Table 2. Deviation of per-panel capacitance from mean value for different PV array configurations.

Array	C_{eq} (nF)	$C_{/\text{panel}}$ (nF)	Error from k (%)
I	60	60	−10.8
II	30	60	−10.8
III	600	85.7	27.3
IV	222	63.4	5.8

3.4 *Quantifying the error*

To quantify the error, per-panel capacitance value is derived from array capacitance values as mentioned in table 1. From these per-panel values, a constant capacitance value is derived based on least-square error from all capacitance values. Taking the constant value as k and the individual per-panel capacitance values from cases mentioned in table 1 as C_1, C_2 etc., error function Π can be formulated as a sum of square of errors:

$$\Pi = (k - C_1)^2 + (k - C_2)^2 + (k - C_3)^2 + (k - C_4)^2. \tag{24}$$

Minimising this error function results in k being the mean of all capacitance values, given by

$$k = \frac{C_1 + C_2 + C_3 + C_4}{4} = 68\,\text{nF}. \tag{25}$$

Deviation from this value, gives the error, which is quantified in table 2. It can be noted that configuration III is a clear outlier and therefore is not considered. Average capacitance value k now comes out to be 61.1 nF. Recalculated errors are reported in table 3. It shows the error to be within 4%.

3.5 *Variation in capacitance with voltage*

The capacitance reported in table 1 is the settled capacitance calculated from second current peak and beyond.

Table 3. Deviation of per-panel capacitance from mean value for different PV array configurations, without the outlier.

Array	C_{eq} (nF)	$C_{/\text{panel}}$ (nF)	Error from k (%)
I	60	60	−1.8
II	30	60	−1.8
IV	222	63.4	3.8

Table 4. Change in array capacitance C_{eq} with voltage V for different PV array configurations.

Array	$C_{eq_{initial}}$ (nF)	$C_{eq_{final}}$ (nF)	ΔV_c (V)	$\frac{\Delta C}{\Delta V}$ (nF/V)
I	104	60	39	1.1
II	67	30	77.3	1.9
III	1200	600	38	2.2
IV	700	220	75	1.8

Table 5. Change in array capacitance C_{eq} with irradiation G for different PV array configurations.

Array	$C_{eq_{lowG}}$ (μF)	$C_{eq_{highG}}$ (μF)	ΔI_{sc} (A)	$\frac{\Delta C_{eq}}{\Delta I_{sc}}$ (μF/A)
III	1.2	1.6	22.8–8.1	0.027
IV	0.7	1.3	29.2–8.4	0.028
V	1.9	2.6	61–40	0.033

However, as mentioned in section 3.1, initial capacitance value is higher as noted from the higher time period between the first two peaks as compared with the subsequent peak time intervals. This is due to the change in PV panel voltage from open-circuit value to zero, which is defined as ΔV. To see the variation in capacitance as a function of voltage, for different PV array configurations, table 4 is presented. It can be observed from table 4 that capacitance variation with voltage is in the range of 1.1–2.2 nF/V per panel. The ratio $\frac{\Delta C}{\Delta V}$ is positive, implying that capacitance increases with voltage. This is in agreement with the reported literature [6].

3.6 *Variation in capacitance with irradiation*

Short-circuit current of a solar cell is an indicative of its irradiation [15]. For the same PV array configuration, capacitance is measured under different light conditions, as indicated by the short-circuit current. The difference in the short-circuit current for these two different light conditions is defined as ΔI_{sc}. The values are tabulated in table 5, where case V represents 14 PV panels connected in parallel. It can be observed from table 5 that the change in capacitance as a function of irradiation is close to 0.03 μF/A; however, exact variation is a function of irradiation value. This sensitivity of capacitance with irradiation is considered in F/A as the short-circuit current level is proportional to the irradiation level [15]. The PV panel capacitance is higher at higher irradiation conditions.

Table 6. Effect of array capacitance on normalised inrush current.

Array	$C_{eq_{initial}}$ (nF)	$\frac{I_{max}}{I_{sc}}$
I	104	3.4
II	67	3.5
III	1200	2.8
IV	700	2.6

3.7 *Effect of capacitance on inrush current*

The effect of equivalent array capacitance on inrush current can be seen by evaluating the ratio of the peak inrush current I_{max} to the short-circuit current I_{sc} value. These variables are marked in figure 6a and their ratio is called as the normalised inrush current. The variation of ratio for different capacitances corresponding to different PV array configurations is shown in table 6. It can be seen that for higher capacitance value, ratio of peak to steady current is lower. Capacitance value is higher for the parallel panel case, where short-circuit current is also higher. Therefore even though the ratio of the peak to the steady current is lower, the absolute value of the peak inrush current is much higher in the parallel connection of PV modules. This observation can be further extended to the irradiation variation of capacitance, wherein it is seen that due to the increase in irradiation, capacitance increases, reducing the peak to steady current ratio. But due to the increase in the short-circuit current, due to the irradiation increase, the absolute value of the peak current is even higher.

4. Limitations in measurements

Practical aspects of the PV array installation cause limitations in the impedance estimation. Voltage and current waveforms are measured at roof bus bar terminal as shown in figure 4. Due to this, the capacitance calculated not only reflects the PV panel capacitance but also includes the effect of cable capacitance. As cable impedance varies for different series and parallel panel connections, direct scalings in inductance and capacitance values were not observed as the cable lengths from the roof top bus bar to individual panels vary. These cables have lengths varying from 2 to 6 m. Therefore these results cannot be

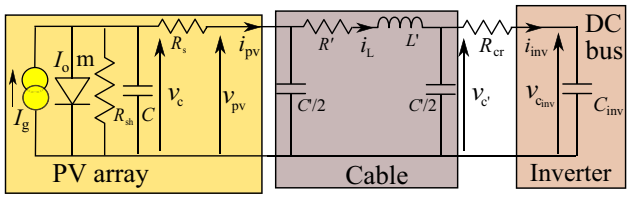

Figure 7. PV array dynamic model, connected to the dc bus of an inverter, via a connecting cable, including contactor resistance.

extrapolated in general; however, the presented method can be used for calculating effective R, L and C values for any system.

5. Refined cable model

In the analysis presented earlier, the connecting cable was modelled by a series impedance of resistance and inductance, similar to a short transmission line, and the cable capacitance was ignored. However, for a frequency range of tens of kHz, the 40 m cable considered can be more accurately modelled using long transmission line equivalent Π circuit [16]. The impedance parameters for this model are evaluated in the appendix. The overall equivalent circuit is presented in figure 7. Due to two additional capacitances, order of the system becomes five. It must be noted that the contactor resistance is modelled as R_{cr} in figure 7. Writing KCL and KVL equations for the circuit shown in figure 7 gives

$$i_L = \frac{C'}{2}\frac{dv_{c'}}{dt} + i_{inv}, \tag{26}$$

$$v_{pv} = v_{c'} + i_L R' + L'\frac{di_L}{dt}, \tag{27}$$

$$i_{pv} = \frac{C'}{2}\frac{dv_{pv}}{dt} + i_L, \tag{28}$$

$$v_c = i_{pv}R_s + v_{pv}, \tag{29}$$

$$i_{pv} = I_g - I_o\left(\exp\left(\frac{v_c}{mn_sV_t}\right) - 1\right) - \frac{v_c}{R_{sh}} - C\frac{dv_c}{dt}, \tag{30}$$

$$i_{inv} = C_{inv}\frac{dv_{inv}}{dt}, \tag{31}$$

$$v_{c'} = i_{inv}R_{cr} + v_{inv}. \tag{32}$$

Similar to the discussion presented in section 2 on small signal model, the present system can be represented with the states of the system as x vector given by $\bar{x} = [v_c \quad v_{pv} \quad i_L \quad v_{c'} \quad v_{inv}]'$ and $\Delta\dot{\bar{x}} = A\bar{x}$ where A is evaluated from (26) to (32) as

$$A = \begin{bmatrix} -\frac{1}{CR_{sh}} - \frac{1}{CR_s} - \frac{I_o e^{\frac{v_c}{mn_sV_T}}}{Cmn_sV_T} & \frac{1}{CR_s} & 0 & 0 & 0 \\ \frac{2}{C'Rs} & -\frac{2}{C'R_s} & -\frac{2}{C'} & 0 & 0 \\ 0 & \frac{1}{L'} & -\frac{R'}{L'} & -\frac{1}{L'} & 0 \\ 0 & 0 & \frac{2}{C'} & -\frac{2}{C'R_{cr}} & \frac{2}{C'R_{cr}} \\ 0 & 0 & 0 & \frac{2}{C_{inv}R_{cr}} & -\frac{2}{C_{inv}R_{cr}} \end{bmatrix}. \tag{33}$$

Substituting the values as obtained from the previous analysis and equivalent Π parameters as reported in the appendix, the eigenvalues of the system can be evaluated. The eigenvalues $e5$ of the matrix (33) are evaluated after removing the non-linearity due to diode, as discussed before in section 2.1:

$$e5 = \begin{bmatrix} 1.12 \times 10^8 \angle 180^\circ \\ 0.13 \times 10^8 \angle 180^\circ \\ 3.82 \times 10^5 \angle 95.7^\circ \\ 3.82 \times 10^5 \angle -95.7^\circ \\ 0.09 \times 10^0 \angle 180^\circ \end{bmatrix}. \tag{34}$$

The eigenvalues, $e3$, for the third-order system represented by (8), come out as follows:

$$e3 = \begin{bmatrix} 4.52 \times 10^5 \angle 95.8^\circ \\ 4.52 \times 10^5 \angle -95.8^\circ \\ 0.09 \times 10^0 \angle 180^\circ \end{bmatrix}. \tag{35}$$

The first two eigenvalues of $e5$ correspond to the small capacitance of the cable; therefore, the large eigenvalues reflect their small time constants. Other three eigenvalues are close for $e5$ and $e3$, which validates that the simplified model as discussed in this paper is reasonably accurate as compared with the more elaborate equivalent Π model. Here eigenvalues are compared, because the eigenvalues of A matrix of a state space model determine the roots of the characteristic equation and therefore eigenvalues of the system determine the dynamics of the system.

5.1 *Variation of system dynamics with cable length and contactor resistance*

Figure 8 shows the locus of the poles of the system with respect to the cable length variation in figure 8a and with respect to the contactor resistance in figure 8b. The eigenvalues are compared for the third-order system marked by blue '+' and for the fifth-order system marked by red 'o'.

5.1a *Effect of cable length*: As the length of the cable is varied, impedance of the cable changes, which further

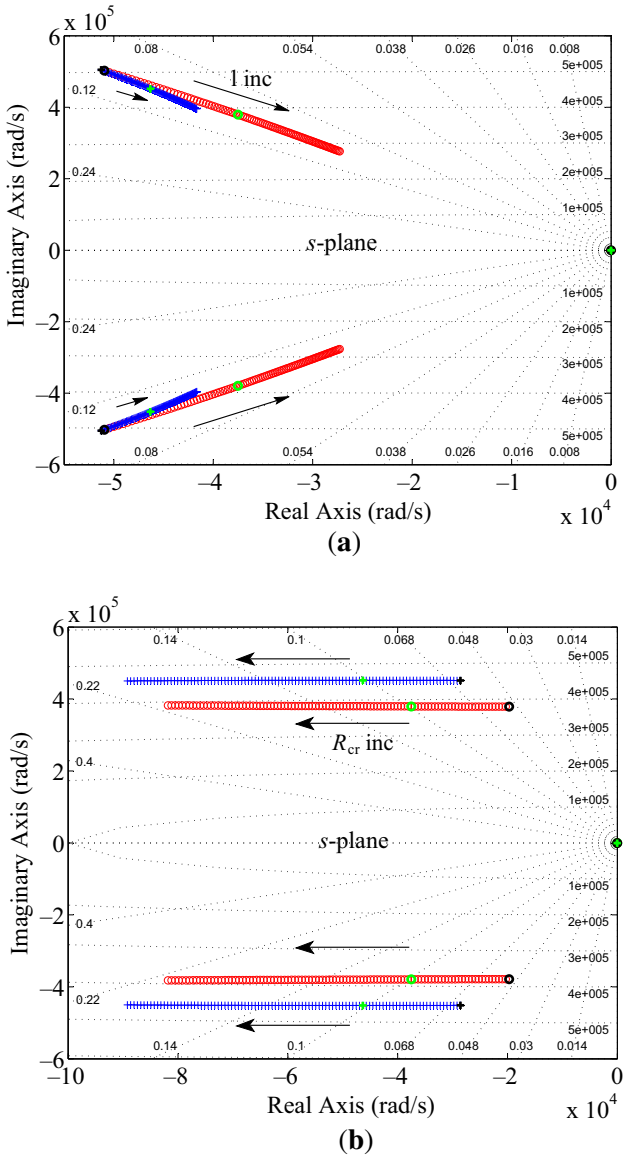

Figure 8. Plot of eigenfrequencies shown for the simplified third-order model and for the fifth-order, refined-cable-based model: (**a**) impact of cable length (1–100 m) on the system eigenfrequencies and (**b**) impact of contactor resistance (0.1–10 Ω) on the system eigenfrequencies.

affects the system dynamics. To capture this, the eigenvalues of the system are plotted against the cable length, which is varied from 1 to 100 m. The results are shown in figure 8a. Only three eigenvalues are compared for the fifth-order system, as the other two eigenvalues were seen to occur at very high frequencies in the left half of *s*-plane. In figure 8a, the present case of 40 m cable length is highlighted with green colour, for both systems. For very low cable length, shown here as 1 m and highlighted with black colour, eigenvalues coincide for third and fifth-order systems. Arrows on the figure mark the direction of increasing cable length from 1 to 100 m, indicating reduction in eigenfrequencies with increasing cable length. From figure 8a, it can be inferred that the damping for both third-order system and the fifth-order system is the same; however, the natural frequency for fifth-order system has a higher variation with cable length as compared with the third-order system. Also the eigenvalue near origin, for both systems, does not change substantially with length.

5.1b *Effect of contactor resistance*: It can be seen from figure 8b that as the contactor resistance increases, damping increases for both third-order and fifth-order systems. Again, only three eigenvalues are compared for the fifth-order system. In figure 8b the present case of 3 Ω contactor resistance is highlighted with green colour, for both systems. For very low contactor resistance, shown here as 0.1 Ω, eigenvalues are highlighted with black colour. Arrows on the figure mark the direction of increasing contactor resistance from 0.1 to 10 Ω, indicating increased damping with increasing contactor resistance.

6. Conclusion

Capacitance of a solar cell is important for dynamic modelling of a PV array. The capacitance is estimated based on experimental measurements. An external capacitor is connected across the terminals of a PV array. This produces a second-order response, the validity of which is checked using a small-signal model. From the second-order response, cable resistance, inductance and PV array capacitance have been calculated. It has been observed that resistance, inductance and capacitance values scale up and down, depending upon the series and parallel combination of PV panels. However, due to the effect of connecting cable impedance, exact scaling is not observed. PV capacitance is seen to change with irradiation at the rate of 30 nF/A, where short circuit current of the PV array is used to indicate the irradiation level. Effect of voltage variation is also seen on the capacitance of PV array, which varies from 1.1 to 2.2 nF/V, depending on the voltage level and array configuration. Due to high open-circuit voltage, capacitance is seen to be higher initially and it is this capacitance value that determines the peak value of the inrush current. The analysis and parameter measurements have been carried out on a variety of PV array configurations and the results are observed to be consistent. The effect of connecting cable capacitance is included to further refine the analysis and is seen to give consistent results with the simplified model.

This analysis can be further extended to derive the analytical expressions of inrush current and PV terminal voltage, when the PV system is connected to a power electronic inverter.

Acknowledgements

This work was supported by CPRI, Ministry of Power, Government of India, under the project "Power conversion, control, and protection technologies for microgrid."

Appendix

A long transmission line can be represented by its equivalent Π network as shown in figure 9 [16]. In this model the equivalent impedance and admittance are given by Z' and Y', respectively:

$$Z' = \frac{Z \sinh(\gamma l)}{\gamma l} \tag{36}$$

$$Y' = \frac{Y \tanh\left(\frac{\gamma l}{2}\right)}{\frac{\gamma l}{2}} \tag{37}$$

where $Y = y \times l$ and $Z = z \times l$, the length of the cable is given by l, z represents the impedance per unit length and y is the admittance per unit length of the cable. The propagation constant is given by $\gamma = \sqrt{y \times z}$. For the 16 mm^2, 1100 V PVC cable used, impedance of the cable, per unit length, is given in its datasheet as follows:

$$r = 1.15\,\text{m}\Omega/\text{m}, \tag{38}$$

$$l = 0.116\,\text{m}\Omega/\text{m}\ @50\,\text{Hz}, \tag{39}$$

$$c = 0.97\,\text{nF/m}. \tag{40}$$

Frequency of interest in the present analysis is in tens of kHz. For a single-panel case, ringing at 50 kHz is observed. Evaluating γ at this frequency, $\gamma = 0.24j$ is obtained. Substituting these values in (36) and (37) for a 40 m cable,

$$Z' = 0.990Z = 0.046 + 4.6j, \tag{41}$$

$$Y' = 1.005Y = 12.26j. \tag{42}$$

However, this value of cable impedance is valid for 50 Hz. For evaluating the actual cable impedance at high frequencies, a network analyser is used. The network analyser gives the impedance of the cable at different frequencies. From the impedance versus frequency data, the equivalent Π parameters of the cable, namely R', L' and C', are curve-fitted using the Levenberg–Marquardt Algorithm [17, 18]:

$$R' = 60.7\,\text{m}\Omega, \tag{43}$$

$$L' = 16.7\,\mu\text{H}, \tag{44}$$

$$C' = 50.9\,\text{nH}. \tag{45}$$

The afore-mentioned value of inductance is further verified using an LCR meter.

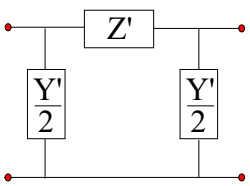

Figure 9. Equivalent Π network of a long transmission line

References

[1] Spertino F, Sumaili J, Andrei H and Chicco G 2013 PV module parameter characterization from the transient charge of an external capacitor. *IEEE J. Photovolt.* 3(4): 1325–1333

[2] Kulkarni A and John V 2016 New start-up scheme for HF transformer link photovoltaic inverter. In: *Proceedings of APEC* pp. 3439–3445

[3] Chen W, Song X, Huang H and Yang X 2014 Numerical and experimental investigation of parasitic edge capacitance for photovoltaic panel. In: *Proceedings of the International Conference on Power Electronics*, pp. 2967–2971

[4] Kumar R A, Suresh M S and Nagaraju J 2001 Measurement of ac parameters of gallium arsenide (GaAs/Ge) solar cell by impedance spectroscopy. *IEEE Trans. Electron Devices* 48(9): 2177–2179

[5] Kim K A, Xu C, Jin L and Krein P T 2013 A dynamic photovoltaic model incorporating capacitive and reverse-bias characteristics. *IEEE J. Photovolt.* 3(4): 1334–1341

[6] Kumar R A, Suresh M S and Nagaraju J 2006 Effect of solar array capacitance on the performance of switching shunt voltage regulator. *IEEE Trans. Power Electron.* 21(2): 543–548

[7] Mauk P H, Tavakolian H and Sites J R 1990 Interpretation of thin-film polycrystalline solar cell capacitance. *IEEE Trans. Electron Devices* 37(2): 422–427

[8] Merhej P, Dallago E and Finarelli D 2010 Effect of capacitance on the output characteristics of solar cells. In: *Proceedings of the 6th Conference Ph.D. Research Microelectronics Electronics*, pages 1–4

[9] Mandal H and Saha S 2015 An improved technique of capacitance measurement of solar cells. In: *Proceedings of the 3rd Conference on Computer, Communication, Control and Information Technology*, pp. 1–4

[10] Recart F and Cuevas A 2006 Application of junction capacitance measurements to the characterization of solar cells. *IEEE Trans. Electron Devices* 53(3): 442–448

[11] Chatterjee A, Keyhani A and Kapoor D 2011 Identification of photovoltaic source models. *IEEE Trans. Energy Convers.* 26(3): 883–889

[12] ABB 2015 *Miniature circuit-breakers S 280 series 80–100 A*

[13] Bharadwaj P, Chaudhury K N and John V 2016 Sequential optimization for PV Panel Parameter Estimation. *IEEE J. Photovolt.* PP(99): 1–8

[14] EMMVEE Photovoltaics 2012 *Photovoltaic module ES 275–295 P72*

[15] Bharadwaj P and John V 2014 Design, fabrication and evaluation of solar irradiation meter. In: *Proceedings of PEDES*, pp. 1–6
[16] Stevenson W D 1982 *Elements of power system analysis*, vol. 196. New York: McGraw-Hill
[17] Chong E K P and Zak S H 2013 *An introduction to optimization*, vol. 76, 2nd edn. New York: Wiley
[18] R2010a, MATLAB 7.10.0. *lsqnonlin*